STUDIA UBB CHEMIA, LXXI, 2, 2026 (p. 209-225)
(RECOMMENDED CITATION)
DOI:10.24193/subbchem.2026.2.11

COMPUTATIONAL AND WATER ELECTROLYSIS STUDY OF 5,10,15,20-TETRAKIS(3-HYDROXYPHENYL)-PORPHYRIN

Marina Alexandra TUDORAN[a], Bogdan-Ovidiu TARANU[a,*]

ABSTRACT. The free-base, symmetrically substituted 5,10,15,20-tetrakis(3-hydroxyphenyl)-porphyrin was the subject of a study combining computational and experimental analysis, with an emphasis on the molecule's water-splitting electrocatalytic characteristics. Ab initio and DFT methods were used to investigate the porphyrin's structural and electronic properties. The water-splitting experiments, performed in solutions with different pH values, were carried out with porphyrin-based electrodes that were modified using different strategies. The electrode manufactured by drop-casting a catalyst ink containing the porphyrin and carbon black on a graphite substrate displayed an overpotential value for the oxygen evolution reaction of 0.595 V *vs.* RHE and a Tafel slope of 0.337 V/dec in a neutral environment. Data acquired during the electrochemical experiments were used to perform statistical analysis. The correlation analysis indicated a significant association between pH and overpotential. The combined study improves the current scientific understanding of the porphyrin's properties and shows the effect of the electrode modification strategies on its water-splitting electrocatalytic activity.

Keywords: *quantum chemical calculations, electrocatalyst, aggregate, water-splitting, oxygen evolution reaction, correlation analysis.*

INTRODUCTION

High energy prices and environmental issues, such as air pollution, are pressing concerns that have led the scientific community to consider hydrogen as a clean energy alternative [1]. Out of several methods for

[a] *National Institute of Research and Development for Electrochemistry and Condensed Matter, Dr. Aurel Paunescu Podeanu Street No. 144, RO-300569, Timisoara, Romania*
* *Corresponding author: b.taranu84@gmail.com*

©2026 STUDIA UBB CHEMIA. Published by Babeş-Bolyai University.
This work is licensed under a Creative Commons Attribution-NonCommercial-NoDerivatives 4.0 International License.

obtaining hydrogen, the most common ones are steam-methane reforming and electrochemical water-splitting (or water electrolysis) [2]. The latter, consisting of the splitting of the water molecule using electricity, is the method upon which green hydrogen production is primarily based [3].

During electrochemical water-splitting, O_2 is produced at the anode via the oxygen evolution half-cell reaction (OER), while H_2 is generated at the cathode through the hydrogen evolution half-cell reaction (HER). One of the main problems facing water electrolysis is the sluggish reaction kinetics of the specified reactions due to high overpotentials [4]. Many materials with electrocatalytic properties have been synthesized and tested in water electrolysis experiments in search of a solution to this issue [5]. The use of inexpensive and earth-abundant catalysts is important for transitioning from a small-scale H_2 production system to a large-scale one [6]. Platinum and IrO_2 are currently the benchmark electrocatalysts for evaluating the performance of other catalytic materials, but their scarcity and high cost prevent large-scale application. The organic tetrapyrrolic structures known as porphyrins are among the more accessible classes of compounds that have been found to possess water-splitting electrocatalytic properties. They exist naturally but can also be synthesized. They share a macrocyclic configuration and constitute extended aromatic systems with amphoteric properties that can be substituted with a wide variety of functional moieties [7]. The various ways in which the porphyrin macromolecule can be modified lead to structures with versatile properties and high applicative potential [8]. The current relevance of porphyrins as water-splitting electrocatalysts is outlined by studies reported in the past few years [9-11]. Porphyrins are also known for their stability in a wide pH range and ability to self-assemble through non-covalent interactions, resulting in aggregates with properties quite distinct from the ones possessed by the molecules comprising them [8].

The current paper presents an integrated investigation of the A_4 free-base 5,10,15,20-tetrakis(3-hydroxyphenyl)-porphyrin. The first part is relevant to the computational chemistry domain, while the second part focuses on the porphyrin's applicative potential in water electrolysis. The molecule was the focus of several studies reported in the literature [12-16], but these are not concerned with its electrochemical water-splitting activity. The results of the electrochemical experiments reveal the porphyrin's properties for water electrolysis in environments with different pH values, complement its current scientific understanding, and outline the effect of different electrode modification strategies on its OER and HER electrocatalytic activity.

RESULTS AND DISCUSSION

Part 1. Theoretical analysis

The optimized molecular structure of 5,10,15,20-tetrakis(3-hydroxyphenyl)-porphyrin is presented in Figure S1 (Supplementary Material file). Data regarding the structural parameters (bond lengths, bond angles, and dihedral angles) are presented in Table S1. These findings confirm the mild conjugative interaction observed between the porphyrin ring and the phenyl ring, which influence the electrochemical behavior of 5,10,15,20-tetrakis(3-hydroxyphenyl)-porphyrin [17,18]. Natural bond orbital analysis is based on the virtual and filled orbital spaces. It can be used to investigate bonding characteristics, charge transfer, and conjugative interaction phenomena in molecular systems [19-21]. The results obtained for the studied molecule are presented in Table S2.

Figure S2 depicts the molecular orbital diagrams for HOMO-1, HOMO, LUMO, and LUMO+1 calculated using the B3LYP functional method. Their corresponding energies are presented in Table S3. In case of 5,10,15,20-tetrakis(3-hydroxyphenyl)-porphyrin, the HOMO–1, HOMO, LUMO, and LUMO+1 electron density is primarily localized on the porphyrin macrocycle, indicating that the frontier molecular orbitals are largely π-conjugated over the core structure. Such delocalization is consistent with the redox behavior of porphyrins, in which a higher degree of conjugation facilitates electron transfer with limited structural reorganization upon oxidation or reduction [18]. Additional data regarding global reactivity descriptors are provided in Table S3.

The analysis of charge localization patterns was conducted using the electrostatic potential map for the molecule in the gas phase (Figure S3). The uneven charge distribution observed for the 5,10,15,20-tetrakis(3-hydroxyphenyl)-porphyrin is important in determining nonlinear optical (NLO) properties, as it shows the extent to which electrons are able to diffuse within the molecule [19]. The NLO properties were investigated, and the results are provided in Tables S4 and S5. Literature reports that a high value of the first hyperpolarizability, as observed for 5,10,15,20-tetrakis(3-hydroxyphenyl)-porphyrin, may indicate electron cloud delocalization within a conjugated framework, involving charge transfer from electron-donor to electron-acceptor groups [22].

Part 2. Water-splitting experiments

Study of the electrodes manufactured using the first modification strategy. The anodic and cathodic polarization curves recorded on the electrodes obtained with the first modification strategy described in the Experimental Section and tested in the acidic medium are shown in Figures S4 and S5 of the Supplementary Material file. Regarding the OER (Figure S4), the linear sweep voltammograms (LSVs) recorded on the modified electrodes and on an unmodified GC sample (GC_0) reveal that GC_0 was more electrocatalytically active. The only exception was the $GC_{P1\text{-}PhCN\text{-}1}$ electrode, in the sense that its activity was more similar to that of GC_0 (Figure S4a). Concerning the HER (Figure S5), all the porphyrin-based electrodes exhibited a lower electrocatalytic activity compared to GC_0. Furthermore, the increase in the number of drop-casted porphyrin layers did not improve the water-splitting properties of the modified samples. Figure S10 displays the heat maps of the calculated OER and HER overpotentials at current densities of 1 and -1 mA/cm², respectively, for the electrodes studied in the acidic medium.

Better results were obtained in the neutral medium, where the OER activity of some modified electrodes was higher than that of GC_0. Figure 1 shows the anodic polarization curves recorded on the electrodes manufactured using the first strategy detailed in the Experimental Section. The highest OER activity was exhibited by $GC_{P1\text{-}PhCN\text{-}1}$ (Figure 1a).

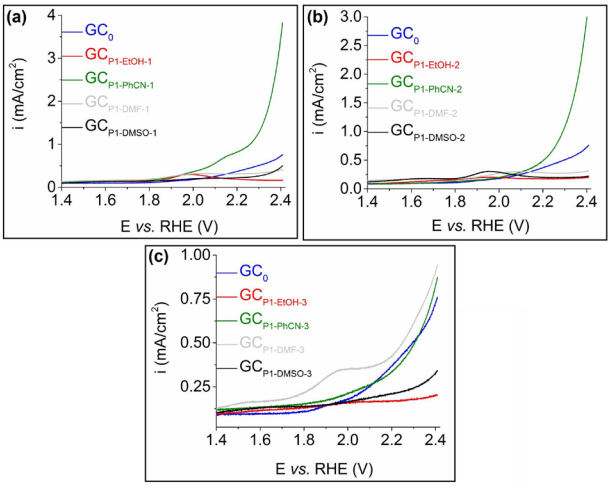

Figure 1. Anodic polarization curves recorded on GC_0 and on (a) $GC_{P1\text{-}EtOH\text{-}1}$, $GC_{P1\text{-}PhCN\text{-}1}$, $GC_{P1\text{-}DMF\text{-}1}$ and $GC_{P1\text{-}DMSO\text{-}1}$; (b) $GC_{P1\text{-}EtOH\text{-}2}$, $GC_{P1\text{-}PhCN\text{-}2}$, $GC_{P1\text{-}DMF\text{-}2}$ and $GC_{P1\text{-}DMSO\text{-}2}$ and (c) $GC_{P1\text{-}EtOH\text{-}3}$, $GC_{P1\text{-}PhCN\text{-}3}$, $GC_{P1\text{-}DMF\text{-}3}$ and $GC_{P1\text{-}DMSO\text{-}3}$. Electrolyte solution: 0.1 M KCl. v = 5 mV/s.

Regarding the HER catalytic activity of the electrodes immersed in the same medium (Figure S6), it was lower than that of GC_0, with the exception of $GC_{P1\text{-}PhCN\text{-}1}$. As shown in Figure S6a, the specified electrode exhibited similar activity to GC_0.

Figure S11 displays the heat maps of the calculated OER and HER overpotentials at current densities of 1 and -1 mA/cm², respectively, for the electrodes studied in the neutral electrolyte solution.

Statistical analysis. The relationship between the overpotential and the experimental factors was further investigated using correlation analysis. In the case of OER (Table S6), a moderate positive correlation was observed between overpotential (η_{OER}) and the pH of the electrolyte solution (r = 0.628, p < 0.05, r^2 = 0.394). No significant correlation was observed between η_{OER} and solvent polarity. The findings indicate that increases in pH are associated with higher overpotential, while solvent polarity exerts no measurable influence on the same parameter, given the selected experimental conditions. In the case of HER (Table S7), correlation analysis revealed a moderate negative association between overpotential (η_{HER}) and pH (r = -0.620, p < 0.05, r^2 = 0.384). A moderate correlation was also identified between η_{HER} and solvent polarity, but in the positive direction (r = 0.602, p < 0.05, r^2 = 0.484). These findings imply that pH and solvent polarity exert opposing, yet significant influences: higher pH is associated with lower overpotential, while increased solvent polarity is associated with higher overpotential. The results are consistent with those reported in the literature on multi-step proton-electron transfer reactions, which demonstrate a clear dependence of the overall reaction rate on the pH value. Furthermore, research has shown that changes in pH affect the electrode|electrolyte interface, as well as the kinetics of electrochemical reactions. From a thermodynamic perspective, in specific electrochemical reactions, modifying the pH level can induce a shift in the electrode's thermodynamic equilibrium potential [23,24].

Study of the electrodes manufactured using the second modification strategy. The results obtained during the experiments performed on the porphyrin-based electrodes modified with the second strategy presented in the Experimental Section are shown in Figure S7 and Figure 2a.

The heat maps of the η_{OER} values calculated at the current densities of 5 and 10 mA/cm^2, as well as the η_{HER} values determined at the current densities of -5 and -10 mA/cm^2, for the electrodes studied in the acidic and neutral electrolyte solutions are presented in Figure S12 and Figure S13, respectively.

Data acquired in the acidic medium (Figures S7a and S7b) indicate that the OER and HER electrocatalytic activity of the porphyrin-containing electrodes was lower than that of the GC_{CB} electrode, manufactured using a GC pellet and a catalyst ink containing 10 mg Carbon Black, 50 µL Nafion solution, and 450 µL double-distilled water. The same situation is observed in the case of the HER results obtained for the neutral medium (Figure S7c). However, the OER data acquired for the same electrolyte solution (Figure 2a) show that O_2 evolved on the $GC_{P1\text{-}CB}$ sample at lower potential values than on the other studied electrodes. To improve the OER activity, the substrate was replaced with spectroscopic graphite [25,26]. Graphite pellets were modified with the second strategy presented in the Experimental Section, and Figure 3b shows the LSVs recorded on the obtained electrodes and on an unmodified graphite pellet (Gr_0). At i = 10 mA/cm^2, the current density value at which η_{OER} is usually determined in water electrolysis studies [27], a η_{OER} value of 0.595 V was found for the $Gr_{P1\text{-}CB}$ electrode. Because of its higher electrocatalytic activity, GrP1-CB was selected for further electrochemical evaluation.

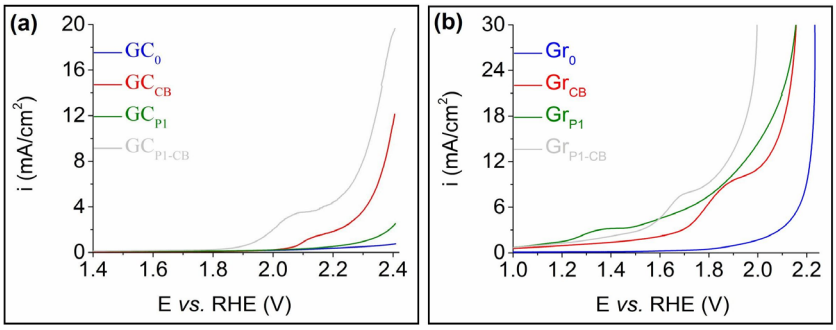

Figure 2. Anodic polarization curves recorded on (a) GC_0, GC_{CB}, GC_{P1} and $GC_{P1\text{-}CB}$ and (b) Gr_0, Gr_{CB}, Gr_{P1} and $Gr_{P1\text{-}CB}$. Electrolyte solution: 0.1 M KCl. *v* = 5 mV/s.

Figure 3 shows the results obtained on $Gr_{P1\text{-}CB}$ by performing additional experiments aimed at revealing more of the electrode's electrochemical properties.

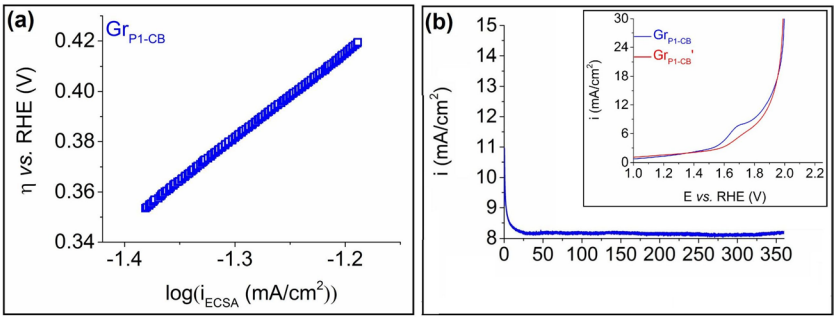

Figure 3. (a) The Tafel plot for $Gr_{P1\text{-}CB}$ in 0.1 M KCl solution. The current density (i_{ECSA}) values from the plot are ECSA-normalized. (b) Amperogram obtained on $Gr_{P1\text{-}CB}$ in 0.1 M KCl solution and inset with the LSVs obtained on the same electrode before ($Gr_{P1\text{-}CB}$) and after ($Gr_{P1\text{-}CB}$') the electrochemical stability test (0.1 M KCl solution, v = 5 mV/s).

The OER kinetics at the electrode:electrolyte solution interface were studied using the Tafel plot shown in Figure 3a. The current density values were obtained by considering the electrode's electrochemically active surface area (ECSA). The value of this parameter, of 27.67 cm^2, was estimated using the method described in the Supplementary Material file, Figure S8, and Equations (S8) and (S9). The Tafel slope of 0.337 V/dec (R^2 = 0.9998) was determined using the Tafel equation, specified as Equation (S10).

Lastly, the $Gr_{P1\text{-}CB}$ electrode was tested in terms of its electrochemical stability over time. The chronoamperogram in Figure 3b was recorded at a constant potential value of 0.595 V *vs.* RHE. The current density reached a value of ~ 8.1 mA/cm^2 after 30 min and remained almost constant throughout the rest of the experiment. The polarization curves obtained before and after the test can be seen in the inset of Figure 3b. The η_{OER} value at i = 10 mA cm^{-2} increased by 35 mV, but no change in the OER overpotential was found in the higher current density region. Raman analysis was performed to verify if the experiment led to structural modifications, and the recorded Raman spectra are shown in Figure S9. The signals visible on the spectrum obtained before the electrochemical stability test are also visible on the one recorded after the test. This indicates the absence of any significant modifications in the chemical structure of the materials at the surface of the modified electrode.

Observations about the water-splitting properties of $Gr_{P1\text{-}CB}$. Out of the carbon-based electrodes modified with the free-base porphyrin, $Gr_{P1\text{-}CB}$ exhibits the highest OER activity. It catalyzes this electrochemical water-splitting half-cell reaction in a neutral electrolyte solution, and its electrocatalytic

properties are probably the result of its surface structural characteristics, charge transport effects, and enhanced π-resonance [28]. Several observations regarding this electrode and the electrocatalyst used to obtain it are appropriate.

According to reported studies, the catalytic center of free-base porphyrins is the N_4 site located in the center of their macrocycle [29,30]. Since the investigated molecule is also a free-base porphyrin, it is probable that its N_4 site serves as the catalytic center. It has also been reported that the value of the ECSA parameter is directly proportional to the number of active sites involved in electrochemical processes [31]. The ECSA value estimated for $Gr_{P1\text{-}CB}$ (27.67 cm^2) is significantly higher than its geometric surface (0.28 cm^2), indicating a relatively high number of catalytically active sites. Charge transfer is also an important factor in electrocatalysis, and it unfolds between neighboring porphyrin molecules through non-covalent π-π interactions. However, when the electrode is immersed in an aqueous electrolyte solution, hydrogen bonds may also become involved. Intermolecular H-bonds can form between the functional moieties of adjacent porphyrin molecules through H_2O molecules [29]. The porphyrin's hydroxyl groups have the potential to form such bonds. Furthermore, charge transfer also occurs between the porphyrins and the carbon substrate. The nitrogen atoms of the N_4 site are more electronegative than the carbon atoms of the electrode's substrate, and this leads to the electropositive doping of that substrate [29]. The electronic effects of the substituents that porphyrins are functionalized with influence their water-splitting electrocatalytic activity as well [30]. The OH^- groups located at the porphyrin's *meta*-positions are electron-withdrawing, which means they decrease the macrocycle's electron density [30]. Lastly, catalytic activity is affected by the pH of the electrolyte solution. Out of the three types of environments used in water-splitting studies – acidic, alkaline, and neutral – investigations performed in neutral electrolyte solutions are more challenging, primarily because of the need to improve the sluggish kinetics of water dissociation in neutral pH [32]. In the case of $Gr_{P1\text{-}CB}$, despite the features that improve its catalytic activity - such as a large number of active sites - the neutral pH of the electrolyte solution, and the electron-withdrawing effect of the OH^- functional moieties are probably responsible for the relatively low OER activity.

The OER electrocatalytic activity of $Gr_{P1\text{-}CB}$ was compared with that of various electrodes reported in the scientific literature, especially with porphyrin-modified electrodes. The electrolyte solutions used to investigate them cover a wide pH range: acidic, neutral, near-neutral, and alkaline. The comparison was performed using the values shown in Table 1. Regarding the OER overpotential, of the 46 values reported in the literature, 12 are higher than

the value found for the $Gr_{P1\text{-}CB}$ electrode, and 8 are smaller but comparable (values > 500 V *vs.* RHE). Regarding the Tafel slope, of the 31 values reported in other studies, 7 are > 337 V/dec, and one is smaller but comparable (0.313 V/dec). These results show that $Gr_{P1\text{-}CB}$ has a place among the electrodes documented in the scientific literature.

Table 1. The OER activity of $Gr_{P1\text{-}CB}$, and of other electrodes reported in the scientific literature. The η_{OER} values are read at i = 10 mA/cm^2.

Electrode or electrocatalyst	Environment	η_{OER} (V *vs.* RHE)	OER Tafel slope (V/dec)	Ref.
Fe-porphyrin polymer@carbon paper	1 M KOH	0.506	0.196	[9]
Co-porphyrin polymer@carbon paper	1 M KOH	0.435	0.069	
Ni-porphyrin polymer@carbon paper	1 M KOH	0.424	0.096	
$G_{P1\text{-}DMF\text{-}3}$	1 M KOH	0.780	0.343	[28]
$G_{P2\text{-}BN\text{-}1}$	1 M KOH	0.780	0.350	
$G_{P3\text{-}DCM\text{-}1}$	1 M KOH	0.850	0.340	
ZnTAPP-NA@GC	1 M KOH	-	0.313	[33]
CoTAPP-NA@GC	1 M KOH	0.416	0.068	
CoTcPP/ZrP@GCRDE	0.1 M KOH	0.467	0.076	[34]
$(Co–P)_{0.5}(Fe–P)_{0.5}$/CNT @GCRDE	0.1 M KOH	0.420	-	[35]
3,4,5-OMe-CoP/CNT@GC	1 M KOH	0.482	0.081	[36]
2,4,6-OMe-CoP/CNT@GC	1 M KOH	0.500	0.090	
CoTPP-SD@CFP	1 M KOH	0.670	-	[37]
CoCOP@CFP	1 M KOH	0.350	0.151	
PIZA-1-400@FTO	1 M KOH	0.430	0.052	[38]
CeO_2/PIZA-1-400@FTO	1 M KOH	0.370	0.048	
Co-MPPy-1@RDE	1 M NaOH	0.420	0.058	[39]
rGO/$(Ni^{2+}–THPP/Co^{2+}–THPP)_8$@RDE	1 M KOH	0.330	0.050	[40]
CoP-2ph-CMP-800@GC	1 M KOH	0.370	0.086	[41]
CoP-3ph-CMP-800@GC	1 M KOH	0.410	-	
CoP-4ph-CMP-800@GC	1 M KOH	0.430	-	
$(CoP)_n$-MWCNTs@GC	1 M KOH	0.290 [a]	0.055	[42]
CoP-TIPS/MWCNTs@GC	1 M KOH	0.440 [a]	-	
$G_{CoP\text{-}DMSO\text{-}1}$	0.5 M H_2SO_4	0.510	0.270	[43]
$G_{CoP\text{-}CH3CN\text{-}1}$	0.1 M KCl	0.630 [b]	-	
$G_{ZnP\text{-}PhCN\text{-}1}$	0.1 M KCl	0.620 [b]	-	
$G_{ZnP\text{-}PhCN\text{-}1}$	1 M KOH	0.560	-	
Porphvlar-based ink @carbon paper	0.1 M PBS	0.670 [c]	0.485	[44]
$G_{CB\text{-}PZn}$	0.1 M KCl	0.780	0.390	[45]
$G_{P1\text{-}BN}$	1 M KOH	0.730	-	[46]

Electrode or electrocatalyst	Environment	η_{OER} (V *vs.* RHE)	OER Tafel slope (V/dec)	Ref.
$G_{P1\text{-}DMF}$	0.5 M H_2SO_4	0.340	-	
$G_{P2\text{-}DMF}$	0.5 M H_2SO_4	0.470	-	
$V_{0.1}Co_{2.9}O_4$	1 M KOH	0.453	-	[47]
C_{60}-SWCNTs	0.5 M H_2SO_4	0.430	-	[48]
TDA-Trz-POP	0.5 M H_2SO_4	0.410	-	[49]
P-CC	1 M KOH	0.450	-	[50]
NH_4@COF-SO_3	1 M KOH	0.543	0.267	[51]
Pristine-COF	1 M KOH	0.652	0.235	[52]
$Fe_{0.5}Ni_{0.5}O_x$	0.1 M KOH	0.584	0.072	[53]
$(FeCoNiCuZn)Al_2O_4$	1 M KOH	0.430	-	[54]
Co-Sn-Mo-Sb oxides	1 M KOH	0.440	-	[55]
CoSAs-MoS2/TiN NRs	1 M PBS	0.508	0.172	[56]
TiN NRs	1 M PBS	-	0.376	
CoSAs-MoS_2 NSs	1 M PBS	-	0.348	
MoS_2/TiN NRs	1 M PBS	-	0.246	
1/MWCNT@GC	0.1 M PBS	0.790	-	[57]
1/MWCNT/Py-Py@GC	0.1 M PBS	0.650	-	
Cr-doped WSe_2/graphene heterojunction	1 M PBS	0.520	0.113	[58]
Co_9S_8/Ni_3S_2/NF	1 M PBS	0.495	0.226	[59]
CoO domains on $CoSe_2$ nanobelts/Ti mesh	0.5 M PBS	0.510	0.198	[60]
$Gr_{P1\text{-}CB}$	0.1 M KCl	0.595	0.337	This work

[a] at 1 mA/cm^2; [b] at 5 mA/cm^2; [c] at 2.5 mA cm^{-2}

CONCLUSIONS

A metal-free symmetrically substituted A_4 porphyrin was investigated in terms of its water-splitting electrocatalytic properties. Computational methods were used to explore the molecule's structure and behavior. Overall, the results suggest that the molecular conformation favors electron-withdrawing behavior. Porphyrin-based electrodes were manufactured using different modification strategies, and their OER and HER catalytic activities were studied in neutral and acidic electrolyte solutions. The experimental data reveal that the most active electrode is the one obtained by drop-casting the catalyst ink containing the porphyrin and carbon black on the surface of a graphite support. This sample exhibits an OER overpotential of 0.595 V *vs.* RHE (at i = 10 mA/cm^2) and a Tafel slope of 0.337 V/dec, in 0.1 M KCl electrolyte solution. While the electrode is relatively stable in the specified

environment, the high overpotential and Tafel slope values indicate that the simple substrate modification strategy should be replaced with more sophisticated ones. Future studies will consider the use of Pulsed Laser Deposition and MAPLE-based protocols for electrode manufacturing.

The relationship between the OER and HER overpotential, on the one hand, and electrolyte pH and solvent polarity, on the other, was investigated as a first step towards improving the design of future experiments aimed at further revealing the water-splitting electrocatalytic properties of the studied porphyrin.

COMPUTATIONAL AND EXPERIMENTAL SECTION

Computational details. Quantum chemical calculations for 5,10,15,20-tetrakis(3-hydroxyphenyl)-porphyrin were performed with Gaussian 03 [61] and visualized with GaussView 6.0 [62]. Geometry optimization in the gas phase was achieved without symmetry constraints by using the Hartree–Fock (HF) method, and the stationary points were identified as minima by performing a vibrational analysis at the same level of theory. The optimized Hartree-Fock (HF) geometry was used to determine the bond lengths and bond angles, in addition to performing natural bond orbital (NBO) analysis. Single-point calculations were conducted on fully optimized geometries with two different hybrid DFT functionals. B3LYP, which combines the Becke three-parameter exchange functional (B3) with the Lee-Yang-Parr (LYP) generalized gradient correlation functional [63,64], and B3PW91, which combines the Becke three-parameter exchange functional (B3) with the Perdew-Wang 91 (PW91) gradient-corrected correlation functional [65,66]. The two approaches yielded analogous results.

Materials and reagents. The 5,10,15,20-tetrakis(3-hydroxyphenyl)-porphyrin was synthesized using a literature-based method [14]. Briefly, propionic anhydride and *m*-hydroxybenzaldehyde were mixed and dissolved in propionic acid under vigorous stirring and heating to reflux. A solution of pyrrole (four times exceeding the molar amount of aldehyde) in propionic acid was slowly added within 45 min. The vigorous stirring and refluxing continued for two more hours and were followed by cooling the reaction mixture to 23 ± 2 °C. Ethanol (95 %) was added, and the precipitation stage was completed in the presence of hexane. A dark purple powder resulted after filtering and repeated hot water washing. The drying and purification of the powder were the final stages of the porphyrin synthesis. The characterization of the compound by ^{1}H-NMR, UV-Vis, TLC, HPLC, MS, FT-IR, and fluorescence spectroscopy was previously reported by Fagadar-Cosma *et al.* [12,14,15]. The chemical structure of the porphyrin derivative is presented in Scheme 1.

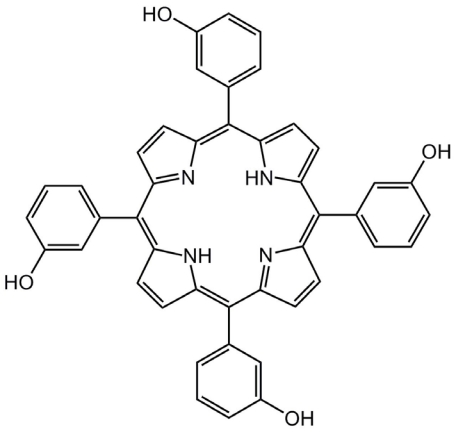

Scheme 1. Chemical structure of 5,10,15,20-tetrakis(3-hydroxyphenyl)-porphyrin.

Benzonitrile (PhCN), dimethylsulfoxide (DMSO), potassium chloride, and sulfuric acid (98 %) were purchased from Merck (Darmstadt, Germany). Ethanol of 99.5 % purity (EtOH) was procured from Honeywell (Charlotte, NC, USA), N,N-dimethylformamide (DMF), and Nafion® 117 solution were acquired from Sigma Aldrich (Saint Louis, MO, USA). The materials used in the study are glassy carbon (GC) pellets purchased from Andreescu Labor & Soft SRL (Bucharest, Romania), SW.114 spectroscopic graphite rods produced at “Kablo Bratislava” (National Corporation “Electrocarbon Topolcany” Factory, Bratislava, Slovakia) and carbon black - Vulcan XC 72 (Fuell Cell Store, Bryan, TX, USA). All aqueous solutions were prepared with double-distilled water from a water distiller (Fistreem, Cambridge, UK). All reagents were used as received without further purification.

Electrode modification strategies. The first protocol for manufacturing porphyrin-based electrodes involved modifying the GC pellets by applying porphyrin solutions of 5 mM concentration to their surface. These solutions were obtained by dissolving the compound in different organic solvents during a 30-minute ultrasonication treatment. The order in which the polarity of the utilized solvents increases is the following: EtOH < PhCN < DMF < DMSO [67]. The procedure for obtaining the modified electrodes consisted in drop-casting a 10 µL volume of porphyrin solution on the surface of the electrically conductive carbon substrate, followed by solvent evaporation at 40 °C. This strategy can be repeated for additional porphyrin layers. Samples with up to three layers were investigated in terms of their OER and HER electrocatalytic activity. The labels used to identify the electrodes are shown in Table 2.

Table 2. Porphyrin-modified electrodes manufactured with the first strategy.

Electrode label	Solvent	Porphyrin layers
$GC_{P1\text{-}EtOH\text{-}1}$	EtOH	1
$GC_{P1\text{-}EtOH\text{-}2}$		2
$GC_{P1\text{-}EtOH\text{-}3}$		3
$GC_{P1\text{-}PhCN\text{-}1}$	PhCN	1
$GC_{P1\text{-}PhCN\text{-}2}$		2
$GC_{P1\text{-}PhCN\text{-}3}$		3
$GC_{P1\text{-}DMF\text{-}1}$	DMF	1
$GC_{P1\text{-}DMF\text{-}2}$		2
$GC_{P1\text{-}DMF\text{-}3}$		3
$GC_{P1\text{-}DMSO\text{-}1}$	DMSO	1
$GC_{P1\text{-}DMSO\text{-}2}$		2
$GC_{P1\text{-}DMSO\text{-}3}$		3

The second protocol for obtaining porphyrin-based electrodes is based on a previously published procedure and involves the deposition of porphyrin-containing catalyst inks on the carbon substrate [68]. Table 3 presents the labeling of the modified electrodes, as well as the compositions of the inks used to manufacture them. These inks were ultrasonicated for 30 min before being drop-casted onto the surface of the pellets (a volume of 10 µL was utilized for each pellet). The electrodes resulted after a drying stage at 40 °C.

Table 3. Porphyrin-modified electrodes manufactured with the second strategy.

Electrode label	Porphyrin amount (mg)	Carbon black (mg)	Nafion solution (µL)	Double-distilled water (µL)
GC_{P1}	10	-	50	450
$GC_{P1\text{-}CB}$	5	5	50	450

Electrochemical investigation. A standard electrolysis setup comprised of a glass cell together with three electrodes connected to a potentiostat (Voltalab PGZ 402 from Radiometer Analytical, Lyon, France) was used throughout the electrochemical study. Each GC-based electrode served as working electrode after insertion into a polyamide support that limited its geometric surface (S_{geom}) to 0.28 cm^2. A Pt plate (S_{geom} = 0.8 cm^2) and the Ag/AgCl(sat. KCl) electrode were utilized as auxiliary and reference electrodes. Since the porphyrin is soluble in alkaline media, the electrolyte

solutions for the experiments were acidic (0.1 M H_2SO_4) and neutral (0.1 M KCl). For the HER investigations, high purity N_2 was used to deaerate the specified solutions. All OER and HER polarization curves were IR-corrected and recorded at the scan rate (*v*) of 5 mV/s [44].

Apart from the mentioned exceptions, the specified current density (i) values refer to the geometric current density. The E values are represented *vs.* RHE (the Reversible Hydrogen Electrode) using Equation (1) [69]. The O_2 and H_2 evolution overpotentials were determined with Equations (2) and (3) [70].

$$E_{RHE} = E_{Ag/AgCl(sat.\ KCl)} + 0.059 \times pH + E°_{Ag/AgCl(sat.\ KCl)} \quad (1)$$

$$\eta_{OER} = E_{RHE} - 1.23 \quad (2)$$

$$\eta_{HER} = |E_{RHE}| - 0 \quad (3)$$

Where E_{RHE} is the converted potential *vs.* RHE (V); $E_{Ag/AgCl(sat.\ KCl)}$ is the measured potential *vs.* the Ag/AgCl(sat. KCl) reference electrode (V); $E°_{Ag/AgCl(sat.\ KCl)}$ = 0.197 V; η_{OER} and η_{HER} are the O_2 and H_2 evolution overpotentials (V).

Statistical analysis. Some of the data obtained during the electrochemical experiments were analyzed using statistical methods. A quantitative evaluation of the overpotential's distribution was carried out using heat maps. Correlation analysis was conducted to assess the relationship between the overpotential and some experimental factors. All statistical calculations were performed using Minitab 22 [71].

Physical-chemical characterization. Raman spectra were acquired with a MultiView-2000 system (Nanonics Imaging Ltd., Jerusalem, Israel) equipped with a Shamrock 500i spectrograph (Andor, Essex, UK).

SUPPLEMENTARY MATERIAL

The Supplementary Material file can be downloaded at:
https://doi.org/10.5281/zenodo.20571954

ACKNOWLEDGMENTS

The authors would like to thank Dr. Eugenia Fagadar-Cosma for providing the porphyrin and Dr. Florina Stefania Rus from INCEMC Timisoara (Romania) for recording the Raman spectra.

REFERENCES

1. A. Dev; V. Kumar; A. S. L. V. Tummala; V. K. Verma; R. Gajjar; A. K. Chaudhary; G. Sarvaiya; B. Parmar; *Discov. Appl. Sci.*, **2025**, *7*, 1336.
2. I. Ali; G. Imanova; O. M. L. Alharbi; A. M. Hameed; M. N. Siddiqui; *J. Umm Al-Qura Univ. Appl. Sci.*, **2023**, *10*, 567-578.
3. H. A. Dhahri; M. Hussain; M. A. A. Ghani; A. Inayat; A. H. Al-Muhtaseb; L. Al-Haj; F. Jamil; *Renew. Sust. Energ. Rev.*, **2026**, *229*, 116617.
4. K.-H. Lin; K.-H. Lee; A. Mukundan; R. Karmakar; E. Rahmawati; K. N. Abdullah; C.-C. Wang; H.-C. Wang; *Energy Rep.*, **2025**, *14*, 5112-5127.
5. Y. Wu; P. Chen; *Green Chem.*, **2026**, *28*, 3043-3072.
6. J. Guo; Y. Haghshenas; Y. Jiao; P. Kumar; B. I. Yakobson; A. Roy; Y. Jiao; K. Regenauer-Lieb; D. Nguyen; Z. Xia; *Adv. Mater.*, **2024**, *36*, 2407102.
7. E. Fagadar-Cosma; D. Vlascici; G. Fagadar-Cosma; *Porfirinele de la Sinteză la Aplicații*; Eurostampa, Timisoara, Romania, **2008**, pp. 10-94.
8. M. Birdeanu; E. Fagadar-Cosma; The self-assembly of porphyrin derivatives into 2D and 3D architectures, in *Quantum nanosystems: Structure, properties and interactions*, M.V. Putz, Ed.; Apple Academic Press, Toronto, Canada, **2014**, Chapter 5, pp. 173-206.
9. N. Ocuane; Y. Ge; C. Sandocal-Pauker; D. Villagran; *Dalton T.*, **2024**, *53*, 2306-2317.
10. I. A. Lane; R. Kumar; *Inorg. Chim. Acta,* **2025**, *576*, 122453.
11. N. Wang; Y. Wang; X. Liu; J. Liu; C. Guo; X. Deng; J. Liang; M. Cao; N. Wang; *Int. J. Hydrogen Energ.*, **2025**, *177*, 151412.
12. E. Fagadar-Cosma; L. Cseh; V. Badea; G. Fagadar-Cosma; D. Vlascici; *Comb. Chem. High T. Scr.*, **2007**, *10*, 466-472.
13. D. Vlascici; E. F. Cosma; E. M. Pica; V. Cosma; O. Bizerea; G. Mihailescu; L. Olenic; *Sensors*, **2008**, *8*, 4995-5004.
14. C. Cretu; C. Bucovicean; I. Armeanu; A. M. Lacrama; E. Fagadar-Cosma; *Rev. Chim.-Bucharest*, **2008**, *59*, 979-981.
15. E. Fagadar-Cosma; M. C. Mirica; I. Balcu; C. Bucovicean; C. Cretu; I. Armeanu; G. Fagadar-Cosma; *Molecules*, **2009**, *14*, 1370-1388.
16. L. Salageanu; D. Muntean; M. Licker; A. Lascu; D. Anghel; E. Fagadar-Cosma; *Farmacia*, **2020**, *68*, 288-298.
17. J. Wang; *J. Phys.: Conf. Ser.*, **2025**, *3008*, 012058.
18. T. T. Tran; M. R. Gan; Y. P. Tzeng; H. Shaw; T. K. Hoang; M. Y. Kuo; Y. O. Su; *J. Electroanal. Chem.*, **2018**, *815*, 40-46.
19. M. Hasnain; S. Urrehman; A. Yousuf; M. A. Ali; T. Fatima; S. Bibi; F. Q. Bai; *Chem. Pap.*, **2025**, *79*, 6809-6824.
20. C. B. Yildiz; Z. O. Sagir; T. Kilic; A. Azizoglu; *Studia UBB Chemia*, **2014**, *59*, 17-32.
21. S. Dhifaoui; A. Azaid; M. Bourass; L. Ben Haj Hassen; H. Nasri; M. Bouachrine; *Phys. Chem. Res.*, **2021**, *9*, 701-713.

22. M. Karabacak; E. Yilan; *Spectrochim. Acta A Mol. Biomol. Spectrosc.*, **2012**, *87*, 273-285.
23. M. T. M. Koper; *Chem. Sci.*, **2013**, *4*, 2710–2723.
24. S. Liu; Z. Wang; S. Qiu; F. Deng; *Carbon Lett.*, **2024**, *34*, 1269-1286.
25. B. O. Taranu; M. G. Ivanovici; P. Svera; P. Vlazan; P. Sfirloaga; M. Poienar; *J. Alloy. Compd.*, **2020**, *848*, 156595.
26. M. Poienar; P. Svera; B.-O. Taranu; C. Ianasi; P. Sfirloaga; G. Buse; P. Veber; P. Vlazan; *Crystals*, **2022**, *12*, 1803.
27. P. W. Menezes; C. Panda; S. Loos; F. Bunschei-Bruns; C. Walter; M. Schwarze; X. Deng; H. Dau; M. Driess; *Energy Environ. Sci.*, **2018**, *11*, 1287-1298.
28. B. O. Taranu; E. Fagadar-Cosma; *Processes*, **2022**, *10*, 611.
29. S. Seo; K. Lee; M. Min; Y. Cho; M. Kim; H. Lee; *Nanoscale*, **2017**, *9*, 3969-3979.
30. W. Zhang; W. Lai; R. Cao; *Chem. Rev.*, **2017**, *117*, 3717-3797.
31. Z. Zhou; W. Q. Zaman; W. Sun; L. M. Cao; M. Tariq; J. Yang; *Chem. Commun.*, **2018**, *54*, 4959-4962.
32. Y. Xu; C. Wang; Y. Huang; J. Fu; *Nano Energ.*, **2021**, *80*, 105545.
33. G. Cai; L. Zeng; L. He; S. Sun; Y. Tong; J. Zhang; *Chem-Asian J.*, **2020**, *15*, 1963-1969.
34. I. B. Alvarez; Y. Wu, J. Sanchez; Y. Ge; M. V. Ramos-Garces; T. Chu; T. F. Jaramillo; J. L. Colon; D. Villagran; *Sustain. Energy Fuels*, **2021**, *5*, 430-437.
35. H. Lei; Q. Zhang; Y. Wang; Y. Gao; Y. Wang; Z. Liang; W. Zhang; R. Cao; *Dalton T.*, **2021**, *50*, 5120-5123.
36. H. Lv; H. Guo; K. Guo; H. Lei; W. Zhang; H. Zheng; Z. Liang; R. Cao; *Chinese Chem. Lett.*, **2021**, *32*, 2841-2845.
37. A. Wang; L. Cheng; W. Zhao; X. Shen; W. Zhu; *J. Colloid Interf. Sci.*, **2020**, *579*, 598-606.
38. D.-J. Li; Z.-G. Gu; W. Zhang; Y. Kang; J. Zhang; *J. Mater. Chem. A*, **2017**, *5*, 20126-20130.
39. S. Bhunia; K. Bhunia; B. C. Patra; S. K. Das; D. Pradhan; A. Bhaumik; A. Pradhan; S. Bhattacharya, *ACS Appl. Mater. Inter.*, **2019**, *11*, 1520-1528.
40. J. Sun; H. Yin; P. Liu; Y. Wang; X. Yao; Z. Tang; H. Zhao; *Chem. Sci.*, **2016**, *7*, 5640-5646.
41. H. Jia; Y. Yao; Y. Gao; D. Lu; P. Du; *Chem. Commun.*, **2016**, *52*, 13483-13486.
42. H. Jia; Z. Sun; D. Jiang; P. Du; *Chem. Mater.*, **2015**, *27*, 4586-4593.
43. B.-O. Taranu, E. Fagadar-Cosma, *Nanomaterials*, **2022**, *12*, 3788.
44. Y. Ge, Z. Lyu, M. Marcos-Hernandez, D. Villagran, *Chem. Sci.,* **2022**, *13* 8597.
45. B.-O. Taranu, F. S. Rus, E. Fagadar-Cosma, *Coatings*, **2024**, *14*, 1048.
46. I. Fratilescu; A. Lascu; B. O. Taranu; C. Epuran; M. Birdeanu; A.-M. Macsim; E. Tanasa; E. Vasile; E. Fagadar-Cosma; *Nanomaterials*, **2022**, *12*, 1930.
47. C. Placke-Yan; G. Bendt; S. Salamon; J. Landers; H. Wende; U. Hagemann; S. Schulz; *Mater. Adv.*, **2024**, *5*, 3482–3489.

48. R. Gao; Q. Dai; F. Du; D. Yan; L. Dai; *J. Am. Chem. Soc.*, **2019**, *141*, 11658-11666.
49. A. Ghosh; M. Mondal; R. N. Manna; A. Bhaumik; *J. Colloid Interface Sci.*, **2024**, *658*, 415-424.
50. Z. Liu; Z. Zhao; Y. Wang; S. Dou; D. Yan; D. Liu; Z. Xia; S. Wang; *Adv. Mater.*, **2017**, *29*, 1606207.
51. Z. Gao; L. L. Gong; X. Q. He; X. M. Su; L. H. Xiao; F. Luo; *Inorg. Chem.*, **2020**, *59*, 4995–5003.
52. Y. Zheng; H. Song; S. Chen; X. Yu; J. Zhu; J. Xu; K. A. I. Zhang; C. Zhang; T. Liu; *Small*, **2020**, *16*, 2004342.
53. J. Jiang; C. Zhang; L. Ai; *Electrochim. Acta*, **2016**, *208*, 17–24.
54. R. R. Katzbaer; F. M. S. Vieira; I. Dabo; Z. Mao; R. E. Schaak; *J. Am. Chem. Soc.*, **2023**, *145*, 6753–6761.
55. A. Pineiro-Garcia; X. Wu; E. J. Canto-Aguilar; A. Kuzhikandathil; M. Rafei; E. Gracia-Espino; *ACS Appl. Mater. Interfaces*, **2024**, *16*, 70429–70441.
56. T. L. L. Doan; D. C. Nguyen; S. Prabhakaran; D. H. Kim; D. T. Tran; N. H. Kim; J. H. Lee; *Adv. Funct. Mater.*, **2021**, *31*, 2100233.
57. I. K. Attatsi; W. Zhu; X. Liang; *New J. Chem.*, **2020**, *44*, 4340-4345.
58. C. H. Chiang; Y. C. Yang; J. W. Lin; Y. C. Lin; P. T. Chen; C. L. Dong; H. M. Lin; K. M. Chan; Y. T. Kao; Suenaga, K.; P.-W. Chiu; C.-W. Chen; *ACS Nano*, **2022**, *16*, 18274–18283.
59. Y. Yang; H. Yao; Z. Yu; S.M. Islam; H. He; M. Yuan; Y. Yue; K. Xu; W. Hao; G. Sun; H. Li; S. Ma; P. Zapol; M. G. Kanatzidis; *J. Am. Chem. Soc.*, **2019**, *141*, 10417–10430.
60. K. Li; J. Zhang; R. Wu; Y. Yu; B. Zhang; *Adv. Sci.*, **2015**, *3*, 1500426.
61. M. J. Frisch; G. W. Trucks; H. B. Schlegel; G. E. Scuseria; M. A. Robb et al.; Gaussian 03, Revision C.02, **2004**, Gaussian, Inc., Wallingford CT.
62. R. Dennington; T. A. Keith; J. M. Millam; GaussView, Version 6.1, **2016**, Semichem Inc., Shawnee Mission, KS.
63. A. D. Becke; *J. Chem. Phys.*, **1993**, *98*, 5648-5652.
64. C. Lee; W. Yang; R. G. Parr; *Phys. Rev. B.*, **1988**, *37*, 785-789.
65. A. D. Becke; *Phys. Rev. A.*, **1993**, *48*, 3098–3100.
66. J. P. Perdew; Y. Wang; *Phys. Rev. B.*, **1992**, *45*, 13244–13249.
67. L. R. Snyder; J. J. Kirkland; J. L. Glajch; Practical HPLC Method Development; John Wiley & Sons, New Jersey, USA, **1997**; pp. 721-728.
68. J. Chang; Q. Lv; G. Li; J. Ge; C. Liu; W. Xing; *Appl. Catal. B-Environmental*, **2017**, *204*, 486-496.
69. B. C. M. Martindale; E. Reisner; *Adv. Energy Mater.*, **2016**, *6*, 1502095.
70. K. Zh. Bekmyrza; K. A. Kuterbekov; A. M. Kabyshev; M. M. Kubenova; A. A. Baratova; N. Aidarbekov; M. D. Chaka; N. E. Benti; *Sci. Rep.*, **2025**, *15*, 28418.
71. Minitab, LLC, **2022**. Minitab (Version 22.x). [Software]. State College, PA, USA: Minitab, LLC.